Polyethyleneimine NH_2-UiO-66 nanofiller-based mixed matrix membranes for natural gas purification

Yuchen Cui [a, #], Xiaolei Cui [a, #], Lubomira Tosheva [b], Chunzheng Wang [a], Yongming Chai [a], Zixi Kang [c], Qiang Gao [d], Kun Wang [c], Zhihan Zhang [a], Hailing Guo [a*], Daohong Xia [a], Daofeng Sun [c]

[a] State Key Laboratory of Heavy Oil Processing, College of Chemical Engineering, China University of Petroleum (East China), Qingdao, Shandong 266580, P.R. China.

[b] Department of Natural Sciences, Manchester Metropolitan University, Chester Street, Manchester M1 5GD, UK.

[c] School of Materials Science and Engineering, China University of Petroleum (East China), Qingdao, Shandong 266580, P.R. China.

[d] School of Chemistry and Chemical Engineering, Qinghai Normal University, Xining 810008, P. R. China.

[#] These authors should be considered co-first authors.

* Corresponding author. guohl@upc.edu.cn (H. Guo)

Abstract

Effective separation of CO_2 from CH_4 is crucial for the purification of natural gas, which requires membrane materials with high permeability, selectivity, and stability of under high pressures. In this work, a high CO_2-affinity MOF-based nanofiller (P_{in}@NH_2-UiO-66) was prepared and integrated in polyetherimide (PEI) to prepare mixed matrix membranes (MMMs) for enhanced CO_2/CH_4 separation capabilities. The P_{in}@NH_2-UiO-66 nanofiller comprised an in situ-formed polyethyleneimine-NH_2-UiO-66 composite prepared via a one-pot synthesis. The polyethyleneimine was covalently attached to the H_2BDC-NH_2 ligand allowing for a stronger integration within the PEI matrix. The polyethyleneimine affects the nucleation of MOF, leading to

miniaturization of the MOF particles. The smaller-sized filler is beneficial for improved interaction at the filler-matrix interface. The numerous amino functionalities grafted onto the NH_2-UiO-66 increased the CO_2 adsorption sites, thereby enhancing the affinity for CO_2. Owing to the improved interaction, the elevated CO_2 attraction, and the inherent properties of the porous NH_2-UiO-66, the fabricated MMMs preformed superior in separating CO_2/CH_4. The 30-P_{in}@NH_2-UiO-66-PEI membrane (containing 30 wt% nanofiller) exhibited a CO_2/CH_4 selectivity of 27.7 and a CO_2 permeability of 2498.9 Barrer. The CO_2 permeability was 21 times greater than that of the pristine PEI membrane, and 4 times higher compared to P@NH_2-UiO-66 MMM with polyethyleneimine modified MOF filler prepared by a traditional wet impregnation method. Additionally, the novel MMM demonstrates excellent separation stability under conditions that mimic industrial settings, demonstrating its potential application for natural gas purification.

Keywords: Mixed-matrix membrane; NH_2-UiO-66; MOF nano-filler modification; CO_2 separation; in situ formation

1. Introduction

Recently, the development of technologies for CO_2 separation from natural gas has attracted considerable attention [1, 2]. The membrane separation technique [3-5] is recognized as one of the most feasible strategies to purify natural gas [6, 7], due to the minimal operational expenses, energy-efficient operation, and decreased carbon emissions. Industrial membranes for natural gas purification should operate effectively at temperatures of about 50 °C (the outlet temperature of a natural gas pipeline) and at elevated gas pressures, and consistently maintain high CO_2 permeability, selectivity and stability [2, 8]. Polymeric membranes currently predominate the membrane market due to their low cost and large-scale manufacturing. The cellulose acetate membrane developed by UOP is the most widely used membrane material in all membrane natural gas processing plants, with a selectivity of 10−15 [9]. However, there are several issues with acid cellulose membranes, including susceptibility to hydrolysis, inadequate permeability and selectivity. Freshly-made thin composite membranes often lose 25%

of their permeability within a week. The balance between permeability and selectivity of polymeric membranes remains challenging, along with maintaining the membrane's structural stability for effective CO_2 separation [10-12]. To tackle these challenges, diverse permeable fillers have been integrated into the polymer matrix to create mixed matrix membrane (MMM) [13-15].

In MMMs, the porous filler is crucial for enhancing CO_2 separation performance by creating pathways for low-resistance transport [15-19]. Among these fillers, metal-organic frameworks (MOFs) stand out as auspicious options, ascribed to the large surface areas and controllable porosity for CO_2 separation [20, 21]. However, improving interaction at the filler-matrix interface is challenging due to the intrinsic differences between organic polymers and MOFs. Moreover, the CO_2-binding property of the MOF fillers exerts a significant role in determining membrane performance. Therefore, it is essential to design MOF fillers that possess superior CO_2 adsorption properties and exhibit strong affinity with the polymer matrix [22].

Plenty research have been dedicated to directed towards advancing the performance of new-generation membranes by tuning the chemical affinity towards CO_2 [14, 23-28]. Amines interacting with open metal sites in MOFs effectively boost the CO_2 uptake at low pressures via furnishing extra adsorption sites [20, 29]. Polyethyleneimine stands out as a highly suitable choice for improving the CO_2 adsorption capabilities of MOFs, as it is rich in amino groups, particularly the primary amine sites located at the chain ends [26, 30, 31]. Additionally, the combination of organic polyethyleneimine and MOF materials is beneficial for enhanced interaction at the filler-matrix interface [28, 32].

The wet impregnation approach is a conventional method used to modify MOFs with polyethyleneimine. This approach involves the coupling of polyethyleneimine with the metal sites of the MOF through weak binding interactions. Liu et al. synthesized branched polyethyleneimine-functionalized UiO-66 via the wet impregnation approach [32], which served as filler in 6FDA-ODA to prepare MMMs for CO_2/CH_4 separating. This resulted in an enhanced CO_2/CH_4 selectivity of 56.49. In addition, the same group designed a nanocomposite filler (UiO-66-PEI@bmim[Tf_2N]) using UiO-66 decorated

with branched polyethyleneimine via wet impregnation method [33], and the MMMs prepared showed an optimum CO_2/CH_4 selectivity of 59.99. Although polyethyleneimine-modified MOF fillers enhance the separation performance of MMMs, the preparation process of modified MOF fillers usually involves high-temperature anhydrous and oxygen-free environment, which complicates the membrane preparation process. Furthermore, a higher level of amine functionalization would result in a higher CO_2 adsorption as well as an enhanced CO_2 permeance. Notably, in comparison with the wet impregnation technique, the in situ covalent grafting method employs a stronger force, consequently facilitating the filler's ability to bind to a greater number of amino groups. Therefore, seeking a simple strategy to modify MOF fillers by introducing more amino groups without high-temperature processing can significantly reduce operational steps and energy consumption.

Herein, we propose a simple in situ one-pot synthesis strategy for the fabrication of polyethyleneimine-modified NH_2-UiO-66 (P_{in}@NH_2-UiO-66) (Scheme 1). The P_{in}@NH_2-UiO-66 nanofillers were then physically blended with polyetherimide to prepare mixed matrix membranes with an enhanced CO_2 separation performance compared to P@NH_2-UiO-66 fillers prepared by conventional wet impregnation. During the in situ synthesis process, polyethyleneimine and H_2BDC-NH_2 ligands are covalently linked to form nano-sized P_{in}@NH_2-UiO-66 fillers with a higher loading of polyethyleneimine. In contrast, the wet impregnation method relies on weaker interactions between NH_2-UiO-66 and polyethyleneimine, resulting in a lower loading capacity of polyethyleneimine. Nano-fillers with high polyethyleneimine load and small size should have better interfacial compatibility with the polymer matrix and higher CO_2 adsorption capacity. Benefiting from these features of P_{in}@NH_2-UiO-66, the MMMs exhibited outstanding CO_2/CH_4 separation performance. The 30-P_{in}@NH_2-UiO-66-PEI membrane with a 30 wt% of the fillers had a CO_2 permeability of 2498.9 Barrer and a CO_2/CH_4 selectivity of 27.7, with 4 times greater permeability compared to MMMs prepared using conventional wet impregnation P@NH_2-UiO-66 fillers.

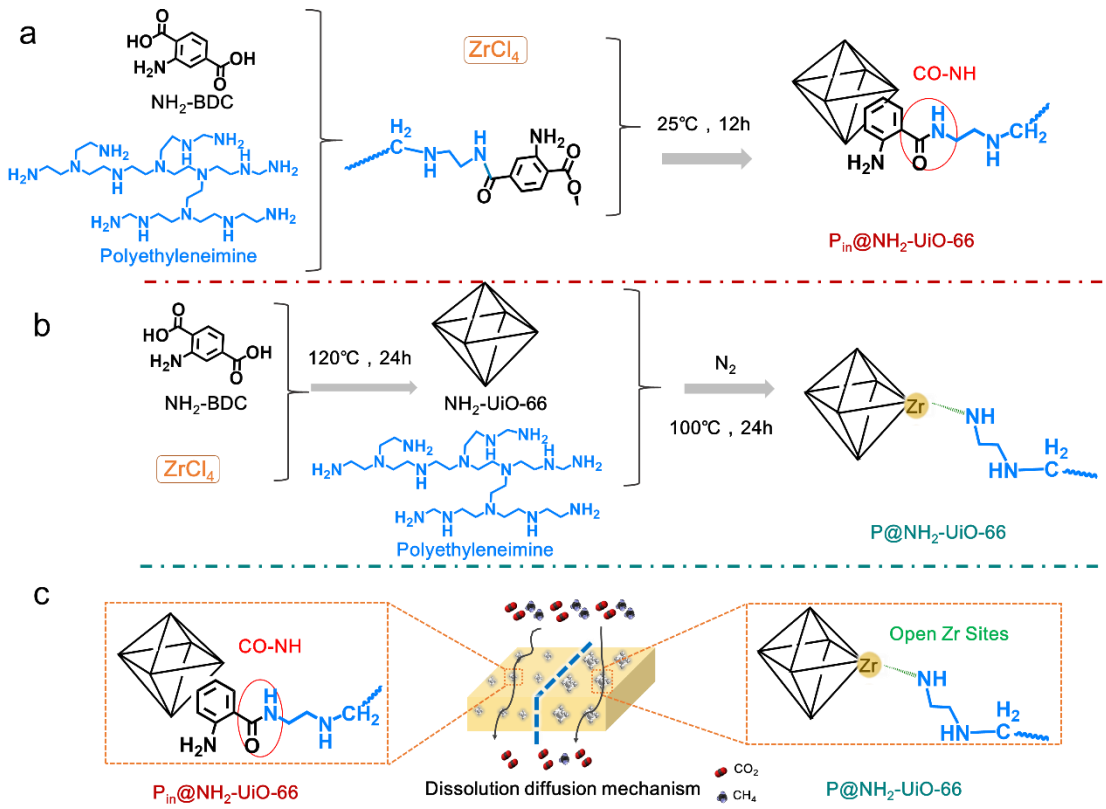

Scheme 1: Schematic illustration for the two preparation methods of mixed-matrix membranes in this work: (a) P_{in}@NH_2-UiO-66 in situ one-pot fabrication process, (b) P@NH_2-UiO-66 wet impregnation synthesis process, (c) membrane processing.

2. Experimental

2.1. Materials

Zirconium (IV) chloride ($ZrCl_4$, 99.5%) powder, formic acid (HCOOH, 88%) and dichloromethane (CH_2Cl_2, 99%) were supplied by Aladdin Biochemical Technology Co., Ltd. (China, Shanghai). 2-Aminoterephthalic acid (H_2BDC-NH_2, 98%) was sourced by Shanghai Macklin Biochemical Co., Ltd, N, N-Dimethylformamide (DMF, 99.8%), Ethanol (CH_3CH_2OH, AR) and methanol (CH_3OH, 99.7%) were supplied by Sinopharm Chemical Reagent Co., Ltd. Polyethyleneimine (99%, W.M. =10000) was supplied by Arkema, France. CH_4 and CO_2 (99.999%) were acquired from Nanjing Special Gases Company. Polyetherimide (PEI) was obtained from SABIC. All compounds employed as received without any other processing.

2.2. Synthesis of NH_2-UiO-66, P@NH_2-UiO-66 and P_{in}@NH_2-UiO-66 nano-fillers

The synthesis of NH_2-UiO-66 was conducted in accordance with established protocols

from previous studies [34]. A mixture of $ZrCl_4$ (4.91 mmol, 1.16 g) and 2-aminoterephthalic acid (4.91 mmol, 0.89 g) was disbursed in 55 mL of dimethylformamide. Subsequently, the mixture was elevated to 120 °C and maintained for 24 h. The obtained NH_2-UiO-66 yellow solid was isolated by centrifugation with dimethylformamide, methyl alcohol and DI water at 5000 rpm for 10 minutes. Afterward, the powder was activated at 60 °C to remove any remaining solvent.

The obtained NH_2-UiO-66 was modified with polyethyleneimine using a wet impregnation method. To eliminate coordinated water, NH_2-UiO-66 particles were heated at 150 °C overnight. Next, 30 mg of polyethyleneimine and 240 mg of NH_2-UiO-66 were separately disbursed in 24 mL methanol under sonication for 10 min. The NH_2-UiO-66 solution was then disbursed to the polyethyleneimine solution slowly while being sonicated. The mixture solution was agitated at 100 °C for 12 hours within a nitrogen environment. Subsequently, the articles were centrifuged and cleaned with absolute ethanol to eliminate solvents. The obtained product called P@NH_2-UiO-66 was dried at 110 °C for 12 h.

Based on the room temperature synthesis of NH_2-UiO-66 [35], 17.5 mL HCOOH was pre-mixed with 160 mL deionized (DI) water containing 1.16 g $ZrCl_4$ under agitation for 15 min. Following this, an additional 0.1 g of polyethyleneimine was incorporated into 50 mL of ethanol with 0.95 g of H_2BDC-NH_2. The blend was then thoroughly mixed for 12 hours at ambient temperature. Upon completion of mixing, a pinkish solid was obtained through centrifugal separation and was further purified by washing with ethanol and deionized water to eliminate contaminants. The product called P_{in}@NH_2-UiO-66 was obtained after drying. NH_2-UiO-66 was prepared in the same way but without the addition of polyethyleneimine and the product was called NH_2-UiO-66-RT.

2.3. Fabrication of MMMs

0.5g Polyetherimide was added to 4.5 g CH_2Cl_2 at room temperature. Following this, the MOF fillers (P@NH_2-UiO-66 and P_{in}@NH_2-UiO-66) were ground and dispersed into the solution to yield a filler content from 10 to 40 wt%. Subsequently, the combined process of 10 minutes of mechanical agitation and ultrasonic treatment were adopted. The casting solutions were subsequently spread onto a clean glass substrate using an automatic membrane applicator to regulate the membrane thickness. Following the application, CH_2Cl_2 solvent was allowed to evaporate completely at ambient condition

for 24 h, followed by additional evaporation periods at 60 °C and 120 °C for 24 h each. Once the solvent was evaporated, the prepared mixed matrix membranes (MMMs) were meticulously stripped from the glass surface. All membranes were reactivated at 120 °C for 24 h prior to gas permeability tests. P@NH_2-UiO-66-based and P_{in}@NH_2-UiO-66-based membranes with different MOFs loadings were labelled as wt%-P@NH_2-UiO-66-PEI and wt%-P_{in}@NH_2-UiO-66-PEI, respectively. As a comparison, 30wt % NH_2-UiO-66 was added as a filler to PEI to make 30-NH_2-UiO-66-PEI membrane.

2.4. Characterization methods

The microstructure and size of the MOF fillers, with the surface properties of the membranes, were investigated using a scanning electron microscopy (SEM, JEOL-7900F) and a transmission electron microscopy (TEM, JEOL JEM-2100UHR). Additionally, X-ray powder diffraction (XRD, Bruker D8 Advance) and Fourier transform infrared (FTIR) spectrometry (Bruker Vertex 70V) were employed to analyze the crystallographic characteristics of both the MOF fillers and the membranes. X-Ray photoelectron spectroscopy (XPS) analysis was carried out via a PH 5000 Versaprobe spectrometer. A Quantachrome Autosorb IQ instrument was carried out to measure N_2 adsorption isotherms at −196 °C. The CO_2 adsorption capacities of MOFs and membranes were also measured by a Quantachrome, Auto sorb IQ instrument at 25°C. The CO_2 and CH_4 adsorption isotherms for the membranes were measured with the Micromeritics ASAP-2020 surface area analyzer at a temperature of 25°C. Thermogravimetric (TGA) and differential scanning calorimetry (DSC) analyses were conducted using NETZSCH (STA 449 F5) to assess the mass loss and glass transition temperature T_g of MMMs, respectively. The nitrogen elemental analysis was performed with a Vario Elementar cube. The kinetic viscosity of the casting solutions was measured by Rheometer (Haake Mars 60).

2.5. Gas-separation tests

The membranes were integrated into a stainless-steel chamber for conditioning, prior to the gas separation experiments. The gas permeability of the membranes was determined using the Wicke-Kallenbach technique, maintaining a feed pressure of 1 bar and a delta pressure across the membrane of 1 bar. The inlet gas was f supplied at a rate of 100 mL min^{-1} (equivalent to 50 cm^3 min^{-1} for each of the binary gas mixtures). A

sweeping argon of 40 cm^3 min^{-1} was applied. For analyzing the composition of the permeated gases, a gas chromatography setup (456-GC, Scion) was employed. Average permeation data were calculated based on measurements from at least three different membranes. The permeability, which is also referred to permeance P_i in Barrer (1 Barrer $=1 \times 10^{-10}$ cm^3 (STP)·cm·cm^{-2} s^{-1}·$cmHg^{-1}$), was calculated using Equation (1) for the membranes:

$$P_i = \frac{10^{-10} l N_i}{A \Delta p_i} \qquad (1)$$

In the specified formula, N_i (cm^3 (STP)·s^{-1}) is the permeate flux, l (cm) denotes the membrane thickness, Δp_i (cmHg) is the pressure difference across the membrane, and A (cm^2) indicates the membrane area.

The separation factor ($\alpha_{i/j}$) of the membrane was calculated based on Equation (2):

$$\alpha_{i/j} = \frac{X_i/X_j}{Y_i/Y_i} \qquad (2)$$

Where X_i/X_j and Y_i/Y_j represent the volume fraction in the permeate gas and feed gas.

The solution-diffusion model was applied to study the gas permeance through the membranes. The calculation formula is shown in Equation (3):

$$P_i l = S_i \times D_i \qquad (3)$$

where the permeability ($P_i l$) is equal to the product of the solubility (S_i, mol m^{-3} Pa^{-1}) and the diffusivity (D_i, m^2 s^{-1}), and l is the thickness of membranes.

The S_i can be calculated by Equation (4):

$$S_i = \frac{C_i}{P} \qquad (4)$$

where C_i (mmol cm^{-3}) and P are the adsorption amount of the membrane for component i and pressure, respectively. D_i was calculated according to Equation (3).

3. Results and discussion

3.1. NH_2-UiO-66, P@NH_2-UiO-66 and P_{in}@NH_2-UiO-66 nano-fillers

XRD analysis (Fig. 1a) showed that NH_2-UiO-66 and P@NH_2-UiO-66 samples exhibit characteristic peaks 7.3° and 8.4° two theta, matching well the simulated NH_2-UiO-66 XRD pattern documented in the previous research [36]. This suggested that the wet impregnation method used for synthesizing P@NH_2-UiO-66 preserves the crystalline arrangement of NH_2-UiO-66. In the case of P_{in}@NH_2-UiO-66 prepared by in situ, one-pot synthesis, the typical NH_2-UiO-66 peaks at 7.3° and 8.4° two theta were observed, together with an amorphous peak in the range 3-12° two theta, indicating the presence of polyethyleneimine in the composite. The crystallinity of NH_2-UiO-66 in P_{in}@NH_2-UiO-66 was calculated via the background constant method [37, 38]. The crystallinity of NH_2-UiO-66 was assessed to be 100%, and the relative crystallinity of P_{in}@NH_2-UiO-66 was found to be 60.4%. During the in situ preparation of P_{in}@NH_2-UiO-66, the introduction of polyethyleneimine interfered with the coordination between the carboxyl groups and the metal zirconium (Zr), thereby affecting the nucleation procedure of NH_2-UiO-66 and leading to a reduced crystallinity.

From the FTIR spectra (Fig. 1b), all samples exhibit a peak at 770 cm^{-1}, associated with the of the Zr-O vibration in NH_2-UiO-66. The -NH- vibration of polyethyleneimine can be seen at 3390 cm^{-1}, indicating the effective grafting of polyethyleneimine onto NH_2-UiO-66. In contrast to P@NH_2-UiO-66, new characteristic peaks of the amide bond appear in P_{in}@NH_2-UiO-66 at 1658 cm^{-1} [39] and 1593 cm^{-1} [33], primarily arising from the condensation reaction between the carboxyl group in H_2BDC-NH_2 and the amino group in polyethyleneimine [28, 39]. In P@NH_2-UiO-66, the amine groups can bind to open Zr sites as reported [33, 40], however, this interaction is relatively weak, resulting in only modest quantity of polyethyleneimine being grafted onto the NH_2-UiO-66. The robust interaction enables P_{in}@NH_2-UiO-66 to combine a greater quantity of polyethyleneimine compared to P@NH_2-UiO-66. The nitrogen content was determined by elemental analyzer to compare the polyethyleneimine content of the three samples. The nitrogen contents of P_{in}@NH_2-UiO-66, P@NH_2-UiO-66, and NH_2-

UiO-66 were 6.56%, 4.78%, and 4.51%, respectively, indicating that P_{in}@NH_2-UiO-66 binds enhanced polyethyleneimine compared to P@NH_2-UiO-66. The interaction was further examined by XPS (Fig. 1 c and d). The N1s peaks at 400 eV and 401.8 eV correspond to the -NH_2 and -NH groups of NH_2-UiO-66, respectively (Fig. 1c). The emergence of a distinct peak at 399.3 eV in the XPS spectrum corresponds to the amide bonds in P_{in}@NH_2-UiO-66 [41]. Further, the C1s XPS spectra (Fig. 1d) indicate that NH_2-UiO-66 reveals three distinct peaks at 284.5eV, 286 eV and 288.5eV, which are respectively belong to sp^2 C, C-N, and O-C-O groups. The C-N ratio of the two composites increases compared with that of NH_2-UiO-66, with the C-N ratio in P_{in}@NH_2-UiO-66 being higher, confirming that more polyethyleneimine is present in P_{in}@NH_2-UiO-66. Additionally, the characteristic peak of amide carbon was observed at 287.6 eV for P_{in}@NH_2-UiO-66 [42]. The XPS results show that there is a condensation reaction between the amino functional group and the carboxyl functional group to form an amide (-CO-NH-).

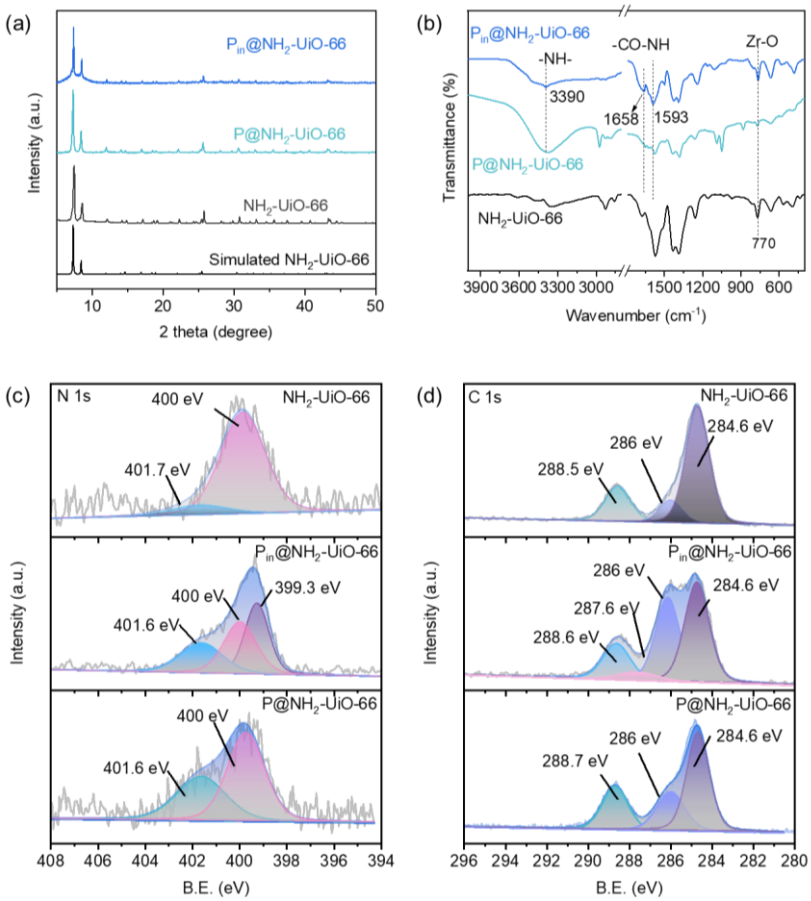

Fig. 1. (a) XRD, (b) FTIR, and (c) XPS N1s analysis and (d) XPS C1s analysis of the as-made NH_2-

UiO-66, P@NH_2-UiO-66, and P_{in}@NH_2-UiO-66 powders.

Fig. 2 exhibits the SEM and TEM images of the as-made NH_2-UiO-66, P@NH_2-UiO-66 and P_{in}@NH_2-UiO-66 powders. The NH_2-UiO-66 nanoparticles exhibit dimensions between 50 and 75 nm, exhibiting a cubic-like shape (Fig. 2a and d), while the P@NH_2-UiO-66 are spherical with particle sizes around 100 nm (Fig. 2b and e). The differences in the shape and size of P@NH_2-UiO-66 nanoparticles are considered to be a result of the encapsulation of polyethyleneimine. The SEM image of NH_2-UiO-66-RT prepared in the absence of polyethyleneimine indicates a cubic-like mosphology of this sample with particle sizes of about 100 nm, and an XRD pattern that matches with the simulated NH_2-UiO-66 (Fig. S1). Relatively, P_{in}@NH_2-UiO-66 consisted of significantly smaller nanoparticles (~ 20 nm) (Fig. 2c and f). The condensation reaction to form amide groups competes for the carboxyl group that should be coordinated with the metal Zr, thus affecting the nucleation process of MOF and leading to the miniaturization of the MOF particles [43]. The reduced particle size of the latter filler enhances the surface area and could improve compatibility with the polymer matrix.

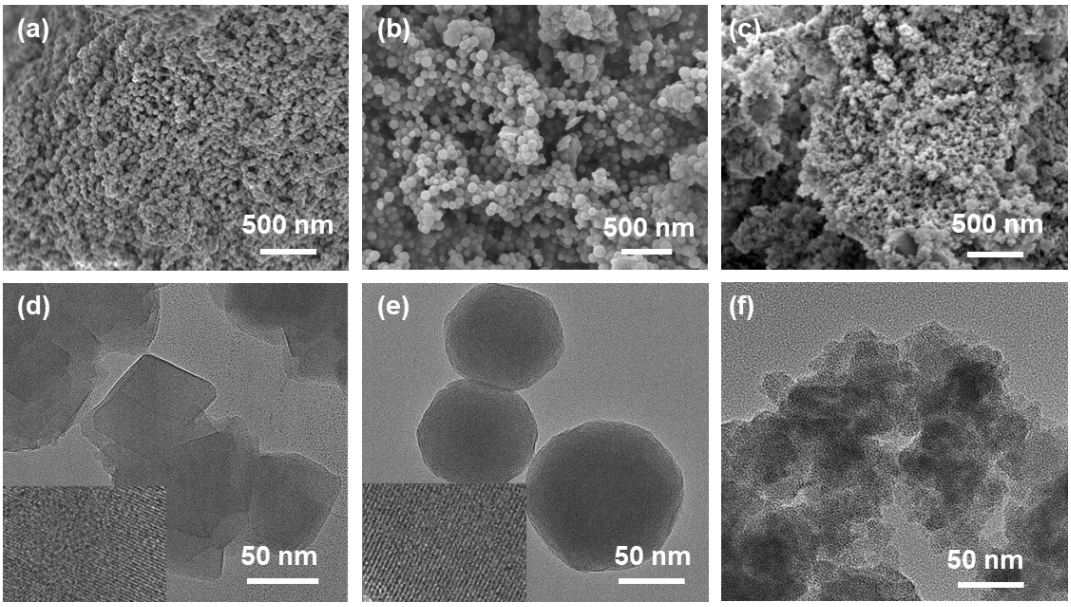

Fig. 2. SEM and TEM images of the as-made (a, d) NH_2-UiO-66, (b, e) P@NH_2-UiO-66, and (c, f) P_{in}@NH_2-UiO-66. The lower left corner of d and e is a high-resolution image.

The N_2 adsorption isotherms of the NH_2-UiO-66, P@NH_2-UiO-66 and P_{in}@NH_2-UiO-

66 all followed hybrid type I and IV isotherms with H4 hysteresis (Fig. S2). Calculated by the t-plot method, the micropore volume of NH_2-UiO-66, P@NH_2-UiO-66 and P_{in}@NH_2-UiO-66 were 0.45 cm^3/g, 0.34 cm^3/g and 0.21 cm^3/g (Table S1). The pore size distribution reveals that the majority of pores measure approximately 0.4-0.6 nm and 1.1 nm. The latter represents the mesopores accumulated by micropores. There are also mesopores that are generated by nanoparticle accumulation in P_{in}@NH_2-UiO-66. While for the P@NH_2-UiO-66, the pore size distribution reveals lower value at around 1.1 nm, indicating less intra-particle mesopores. In addition, there were less mesopores that accumulated by the nanoparticles due to the larger particle size of P@NH_2-UiO-66. The mesopores allow rapid gas diffusion into the pores of fillers, further significantly decrease the trans-membrane mass transfer resistance of the MMMs, which facilitates diffusion processes. Therefore, the diffusion coefficient of P@NH_2-UiO-66-PEI membrane will be lower. The micropore diameters of NH_2-UiO-66 was 0.55 nm, being close to the MOF structure windows of about 6 Å, and the pore size of P@NH_2-UiO-66 and P_{in}@NH_2-UiO-66 reveal a slightly decrease (0.50 and 0.44 nm). The both reduction of pore volume and pore size indicates the occupation of the pores by polyethyleneimine. The P_{in}@NH_2-UiO-66 binds more polyethyleneimine than the P@NH_2-UiO-66, leading to more severe pore plugging.

The thermal stability of P@NH_2-UiO-66 and P_{in}@NH_2-UiO-66 was tested under N_2 atmosphere (Fig. 3). The initial mass decrement observed above 100 °C is assigned to the evaporation of adsorbed H_2O and gases. The step mass loss before 280 °C is attributed to dehydroxylation of the zirconium oxo clusters. The subsequent mass reduction occurring beyond 280 °C is ascribed to the structural collapse of NH_2-UiO-66 [35, 44]. These results show that the P@NH_2-UiO-66 and P_{in}@NH_2-UiO-66 fillers have good thermal stability.

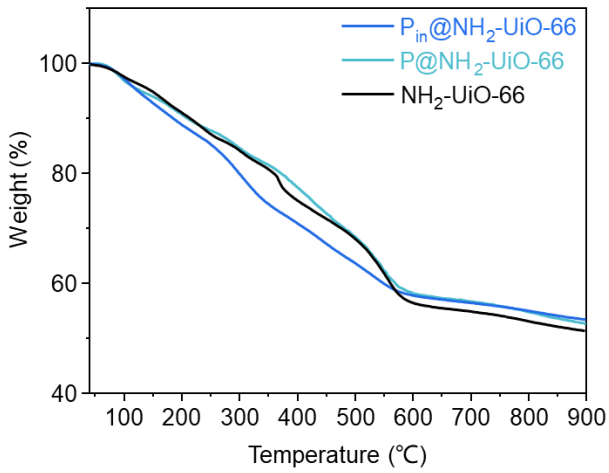

Fig. 3. TGA in N_2 of the as-made NH_2-UiO-66, P@NH_2-UiO-66, and P_{in}@NH_2-UiO-66.

P_{in}@NH_2-UiO-66 and P@NH_2-UiO-66 exhibited CO_2 saturation adsorption capacities of 46 and 35 cm^3g^{-1}, respectively, surpassing that of NH_2-UiO-66 (15 cm^3g^{-1}) (Fig. 4). The increase of CO_2 adsorption was mainly related to the modification of MOF by polyethyleneimine. The grafting of polyethyleneimine with rich amino groups to NH_2-UiO-66 generates additional sites for CO_2 adsorption. Furthermore, from the elemental analysis and XPS results (Fig. 1c, d), P_{in}@NH_2-UiO-66 has a higher polyethyleneimine content, therefore it has the highest CO_2 adsorption capacity. This high CO_2 adsorption capacity is beneficial for the CO_2/CH_4 separation performance of the MMMs.

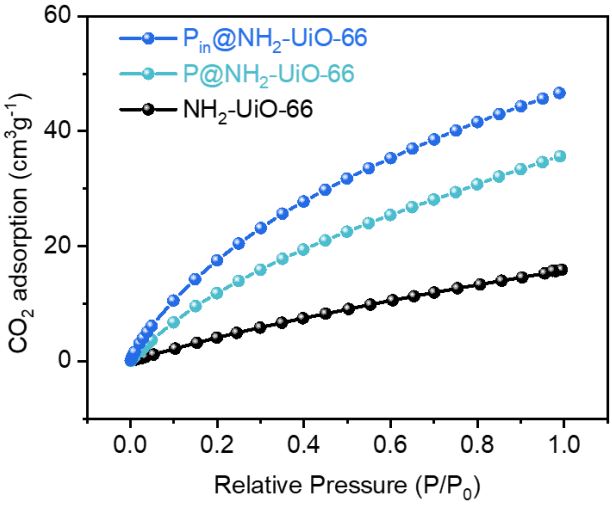

Fig. 4. The CO_2-adsorption curves of the as-made NH_2-UiO-66, P@NH_2-UiO-66, and P_{in}@NH_2-UiO-66.

3.2. Membrane characterization

SEM images in Fig. 5, Fig. S3 and Fig. S4 were applied to characterize the top and cross-sectional structure of the pure PEI, P@NH_2-UiO-66-PEI, and P_{in}@NH_2-UiO-66-PEI membranes. The fabricated MMMs exhibited a substantial surface roughness, which tends to increase with the loading, compared to the PEI membrane (Fig. 5 a-c, Fig. S3 a-e and Fig. S4 a-d). Agglomeration was noticed on the surface of the P@NH_2-UiO-66-PEI membrane (Fig. 5c and Fig. S3), indicating a less-than-ideal distribution of particles throughout the PEI matrix. In the cross-section SEM images (Fig. S3 f-j and Fig. S4 f-j), the thickness of the PEI, P_{in}@NH_2-UiO-66-PEI, and P@NH_2-UiO-66-PEI membranes were determined to be in the range 68-91 μm. For P_{in}@NH_2-UiO-66-PEI, it is evident that P_{in}@NH_2-UiO-66 is enveloped by the polymer chains, forming defect-free microstructures (Fig. 5e and Fig. S4). The emergence of polymer veins serves as additional evidence supporting the existence of robust interfacial interactions [45], while this polymer vein was invisible in P@NH_2-UiO-66 based MMMs (The upper right corner of Fig. 5e and f). The outcome of this effect could be attributable to the presence of interaction forces between the imine groups (–N(R)-H) of the polyethyleneimine and the carbonyl groups (C=O) of the PEI matrix. The EDS mapping in Fig.5g-i shows that the nitrogen content of P_{in}@NH_2-UiO-66-PEI membrane is higher than that of P@NH_2-UiO-66-PEI and pure PEI membranes, further proving the nitrogen content of P_{in}@NH_2-UiO-66-PEI is the highest.

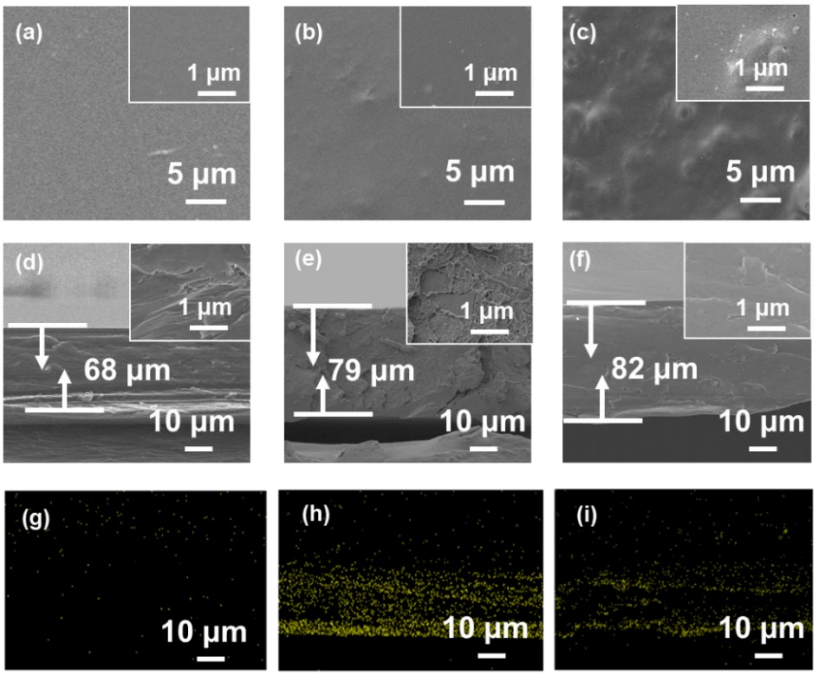

Fig. 5. Top-view SEM images of (a) pure PEI membrane, (b) 30-P_{in}@NH_2-UiO-66-PEI, (c) 20-P@NH_2-UiO-66-PEI, and cross-section SEM images of (d) pure PEI membrane, (e) 30-P_{in}@NH_2-UiO-66-PEI and (f) 20-P@NH_2-UiO-66-PEI (The upper right corner of a-f is the enlarged image), Corresponding elemental mapping images of N ka of (g) pure PEI membrane, (h) 30-P_{in}@NH_2-UiO-66-PEI, (i) 20-P@NH_2-UiO-66-PEI

XRD characterization was conducted to further characterize the structure of as-made membranes. Pristine PEI is a copolymer that features broad peaks centered at 14° two theta (Fig. 6a) [46]. The MOFs preserve their crystallinity and phase within the PEI as seen by the peaks at 7.37° and 8.44° two theta. Fig. S5 a, b displays the XRD patterns of P@NH_2-UiO-66-PEI and P_{in}@NH_2-UiO-66-PEI membranes prepared with different loadings. As the loading of the MOF increased, the intensity of the MOF characteristic peaks (especially at 7.37° and 8.44° two theta) progressively enhanced, indicating that the crystallinity of the nano-filler can be maintained during the membrane preparation process. The d-spacing values were calculated by using the Bragg's law. This value was lower for MMMs (d=5.7-5.9Å) than pristine PEI membrane (d=6.4 Å), as shown in the Fig .S5a, b. Thus form the result, the interaction between filler and polymer matrix increased the rigidity of the membrane, reducing the inter-segmental mobility and d-spacing, and enabling the membrane to allow only small molecules to penetrate through it. Given that the CO_2 molecule (3.6 Å) is smaller in size compared to the CH_4 molecule (3.8 Å), the MMMs potentially facilitates the passage of CO_2 through the membrane, thus enhancing CO_2 permeability.

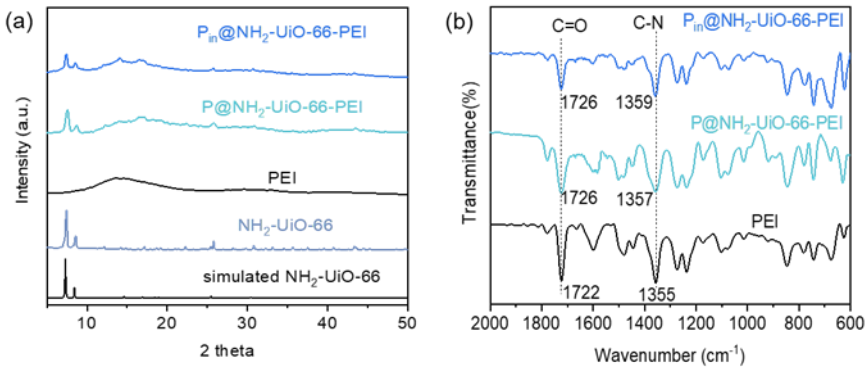

Fig. 6. XRD patterns (a) and FTIR spectra (b) of pristine PEI, P@NH_2-UiO-66-PEI and P_{in}@NH_2-

UiO-66-PEI membranes.

FTIR spectra of the membrane samples (Fig. 6b) were obtained to acquire insight of the interaction between incorporated P@NH_2-UiO-66 or P_{in}@NH_2-UiO-66 MOFs and PEI. The FTIR spectrum of the PEI matches with that described in published studies [47]. The characteristic peaks corresponding to the pristine PEI polymer remain intact in all MMMs, showing no noticeable changes in intensity. As the filler loading increased, the peaks observed at 1780 cm^{-1} (C=O asymmetric), 1722 cm^{-1} (C=O symmetric stretching vibration), and 1355 cm^{-1} (C-N stretch of imide groups) (Fig. S5 c, d), which were slightly red-shifted, and their intensity gradually increased. This could be can be ascribed to the interaction between the amide groups and the carbonyl (C=O) groups of the PEI via hydrogen bonding. P_{in}@NH_2-UiO-66-PEI exhibited enhanced shift, suggesting significantly intensified hydrogen bonds.

The XRD pattern of 30-NH_2-UiO-66-PEI membrane matches with the simulated NH_2-UiO-66 and pure PEI (Fig. S6). The top-view SEM images of 30-NH_2-UiO-66-PEI indicates a rough surface morphology with particles agglomerated. The cross-section SEM images shows obvious interface defects and voids, with membrane thickness of 59 μm.

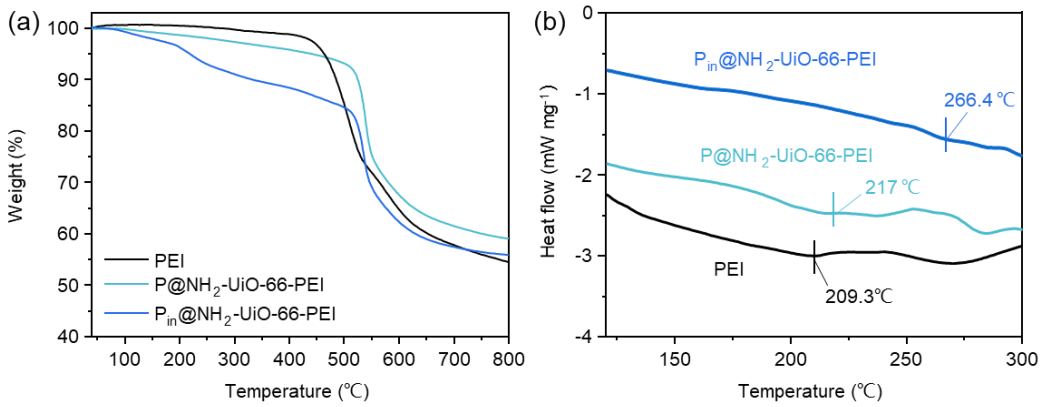

Fig. 7. TGA curves (a) and DSC curves (b) of pristine PEI, P@NH_2-UiO-66-PEI and P_{in}@NH_2-UiO-66-PEI membranes.

The thermal stability of mixed matrix membranes was investigated using thermogravimetric measurements (Fig. 7a). Starting from 200 °C, MMMs experienced

weight loss due to MOF degradation and the decomposing of polyethyleneimine of the fillers. The mass loss begin at 450-500 °C occurred as a result of PEI decarboxylation [46]. The MMMs with P_{in}@NH_2-UiO-66 and P@NH_2-UiO-66 fillers demonstrated a larger residual mass than the pristine PEI, suggesting filler decomposition. The glass transition temperature (T_g) determined by DSC measurements (Fig. 7b and Table.S2) was performed to assess the interaction between the fillers and the PEI. Pristine PEI membrane exhibited a T_g of 209.3 °C which matched well with the literature [48]. The 30-P_{in}@NH_2-UiO-66-PEI exhibited a much higher T_g value (266.4 °C) compared to 20-P@NH_2-UiO-66-PEI (217 °C). The reason is that more amine groups on the P_{in}@NH_2-UiO-66 show stronger hydrogen bonding with the PEI matrix, which indicates that P_{in}@NH_2-UiO-66-PEI have higher chain rigidity with robust interfacial interactions within the membranes. In addition, with the increase of filler content, the T_g of MMM increased, while the T_g of 40-P_{in}@NH_2-UiO-66-PEI membrane decreased slightly, which was due to the fact that overmuch filler was prone to agglomeration in the matrix and weakened the interfacial compatibility.

The viscosity of the casting solutions was measured to further investigate the interactions between the filler and the polymer (Fig. S7). The P_{in}@NH_2-UiO-66-PEI solution exhibited superior viscosity compared to that of the P@NH_2-UiO-66-PEI solution and the PEI polymer, confirming the enhanced interfacial compatibility [49, 50]. The enhanced interface compatibility is beneficial for the selective separation effect of CO_2.

3.3. Gas separation performance

Mixed gas permeation measurements (with CO_2/CH_4 =50/50 by volume) were performed to evaluate the separation capabilities of prepared membranes. Initially, the impact of P@NH_2-UiO-66 and P_{in}@NH_2-UiO-66 loading was examined. (Fig. 8a, b and Table S3). As exhibited in Table S3, the modified Zr-MOF MMMs exhibit higher CO_2 permeability and CO_2/CH_4 selectivity compared to NH_2-UiO-66-PEI. The aggregation caused by the larger crystal size of NH_2-UiO-66 and inhomogeneous distribution results in nonselective voids, leading to the lower selectivity for CO_2/CH_4.

And the low CO_2 saturated adsorption capacity of NH_2-UiO-66 leads to the lower CO_2 permeability. As the increase in both filler loadings, the CO_2 permeability increases, mainly because the introduction of more MOFs provides more gas transport channels for MMMs. Correspondingly, the CO_2/CH_4 selectivity demonstrated a tendency of initial of incremental rise initially, which was succeeded by a decline. The increase of polyethyleneimine load in the membrane introduced more CO_2 adsorption sites, which resulted in higher gas selectivity. When the filler loading was too high, non-selective voids were generated due to nanofiller aggregation (for instance Fig. S3h), reducing the CO_2/CH_4 selectivity. For P_{in}@NH_2-UiO-66-PEI membrane, the MMM with 30% filler loadings exhibited the best performance. The 30-P_{in}@NH_2-UiO-66-PEI membrane exhibited the CO_2 permeability of 2498.9 Barrer with CO_2/CH_4 selectivity of 27.7, respectively. The 20-P@NH_2-UiO-66-PEI demonstrated best results for the P@NH_2-UiO-66 filler with a CO_2 permeability of 484.2 Barrer with CO_2/CH_4 selectivity of 11.4, respectively. The significant difference in separation performance of P_{in}@NH_2-UiO-66 and P@NH_2-UiO-66 based membranes was mainly related to the amount of polyethyleneimine modification. The membranes with higher polyethyleneimine loading capacity showed superior CO_2/CH_4 separation performance.

Fig. 8c revealed that the incorporation of P@NH_2-UiO-66 and P_{in}@NH_2-UiO-66 nano-fillers improved the selectivity and permeability for both gases over the pure PEI membranes. The P_{in}@NH_2-UiO-66-PEI exhibited enhanced CO_2/CH_4 performance compared to P@NH_2-UiO-66-PEI, which was due to the improved CO_2 affinity of P_{in}@NH_2-UiO-66 and better interfacial compatibility the PEI matrix. The CO_2 permeability and CO_2/CH_4 selectivity of the 30-P_{in}@NH_2-UiO-66-PEI membrane was respectively 4 and 2.7 times of the P@NH_2-UiO-66-PEI membrane and much higher than the pure PEI membrane.

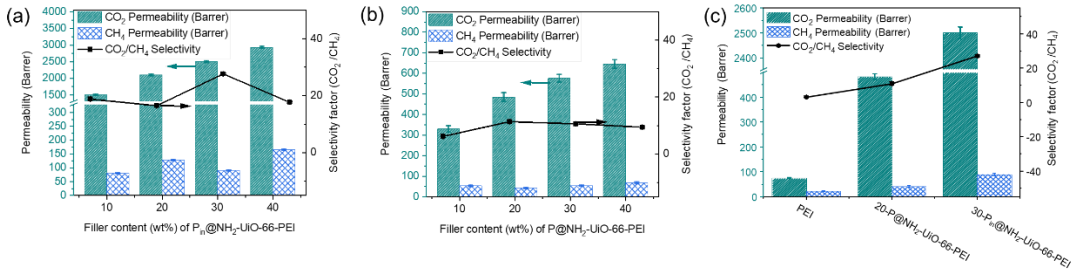

Fig. 8. The effect of fillers loading on the CO_2/CH_4 separation efficiencies of (a) $P_{in}NH_2$-UiO-66-PEI and (b) P@NH_2-UiO-66-PEI membranes. (c) Contrast of CO_2/CH_4 separation efficiencies of PEI, 20-P@NH_2-UiO-66-PEI and 30-$P_{in}NH_2$-UiO-66-PEI membranes.

To illustrate the improvement of CO_2 adsorption capacity of the membranes, the gas adsorption experiments were performed on the P@NH_2-UiO-66-PEI membrane and P_{in}@NH_2-UiO-66-PEI membrane with CO_2 and CH_4 at 298 K (Fig. S8). The adsorption capacities of the P@NH_2-UiO-66-PEI membrane for CO_2 and CH_4 were 10.20 and 3.31 $cm^3\ g^{-1}$ at 298 K, while those of P_{in}@NH_2-UiO-66-PEI membrane for CO_2 and CH_4 were 25.33 and 4.12 $cm^3\ g^{-1}$ at 298 K. The CO_2 adsorption ability of the P_{in}@NH_2-UiO-66-PEI membrane is higher than that of the P@NH_2-UiO-66-PEI membrane, proving that the in-situ modification of polyethyleneimine to the fillers can effectively improve the CO_2 adsorption capacity of the membrane. The solubility (S) and diffusivity (D) for the 30-P_{in}@NH_2-UiO-66-PEI and P@NH_2-UiO-66-PEI membranes are summarized in Table S4. The result shows that the selectivity of the membrane is more dependent on solubility (S_{CO2}/S_{CH4}=6.4 > D_{CO2}/D_{CH4}=4.3). It is much easier to adsorb CO_2 than CH_4 by the 30-P_{in}@NH_2-UiO-66 membranes, declining the adsorption and diffusion of CH_4, thereby enhancing the separation selectivity. The CO_2 solubility of 30-P_{in}@NH_2-UiO-66-PEI membrane shows higher value ($1.2 \times 10^{-8} > 8.2 \times 10^{-9}$) than 30-P@$NH_2$-UiO-66-PEI membrane due to the higher CO_2 adsorption ability of membrane. Furthermore, in contrast to the 30-P_{in}@NH_2-UiO-66-PEI membrane, the CO_2 diffusion of the 30-P@NH_2-UiO-66-PEI membrane shows lower value ($5.3 \times 10^{-6} < 1.1 \times 10^{-5}$), attributed to the reduced presence of mesopores in P@NH_2-UiO-66.

3.4. Influence of temperature, pressure, and feed gas

Fig. 9a assessed the impact of operational temperature within the range of 25–100 °C. For 30-P_{in}@NH_2-UiO-66-PEI membrane, the permeability of CO_2 and CH_4 exhibited a notable enhancement with increasing operational temperature, while the selectivity of CO_2/CH_4 remained at a high level of 19.4. This shows that P_{in}@NH_2-UiO-66-PEI membrane can maintain excellent CO_2/CH_4 separation performance even at high operating temperatures (100 °C).

Examining the impact of transmembrane pressures on the performance of the produced membranes is essential. The observed trend in Fig. 9b indicates that the CO_2 permeability gradually decreases with the transmembrane pressure increases from 1 bar to 10 bar. This can be attributed to that the CO_2 affinity of the membrane approaches saturation with the feed pressure increasing. As a result, the available sites for CO_2 adsorption become limited, leading to a decline in the overall permeability and CO_2/CH_4 selectivity [11, 16]. The CO_2/CH_4 selectivity of the MMMs remains substantially superior to that of the PEI membrane under elevated pressures (e.g. 10 bar, Fig. 9b), emphasizing the enormous potential of these as-made MMMs under operational conditions.

The different feed gas pressure of CO_2/CH_4 mixed gases (50/50, 30/70, and 10/90 by volume) was investigated and the results are shown in Fig. 9c. The CO_2/CH_4 selectivity decreased with the increase of CH_4 permeability due to higher CH_4 feed partial pressure. 30-P_{in}@NH_2-UiO-66-PEI still maintained the CO_2/CH_4 selectivity of 21.3 while a permeability of up to 2116 Barrer in the case of a feed volume ratio of 10/90.

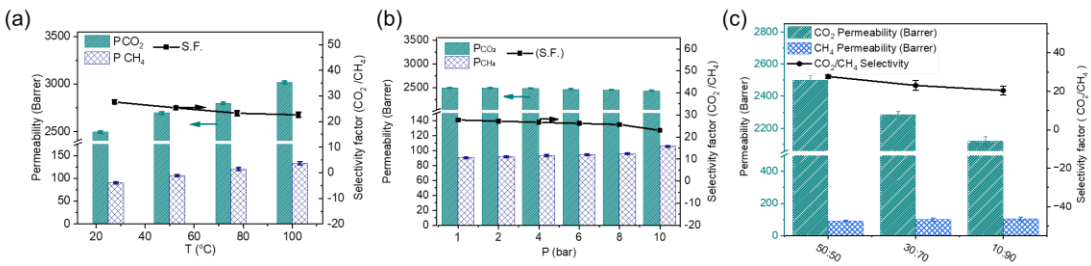

Fig. 9. (a)The effect of operation temperature on CO_2/CH_4 separation performance of 30-P_{in}@NH_2-

UiO-66-PEI at 1 bar. (b)The effect of operation pressures on CO_2/CH_4 separation performance of 30-P_{in}@NH_2-UiO-66-PEI at 25 °C. (c) The effect of different feed gas ratios of the CO_2/CH_4 separation performance of 30-P_{in}@NH_2-UiO-66-PEI at 25 °C and 1 bar.

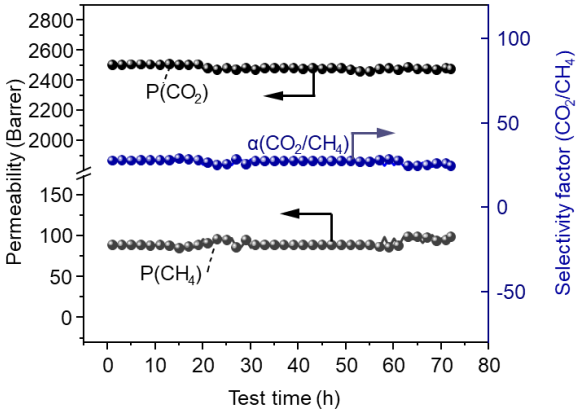

Fig. 10. 72 h operation test of 30-P_{in}@NH_2-UiO-66-PEI.

3.5. Long-term stability

Fig. 10 presents long-term stability test of CO_2/CH_4 separation to assess the stability of the membrane structure. During a 72 h operation test, the 30-P_{in}@NH_2-UiO-66-PEI membrane remained a stable CO_2 permeability of 2498.9 Barrer and a consistent CO_2/CH_4 selectivity of 27.7. Additionally, it confirms that the fabricated 30-P_{in}@NH_2-UiO-66-PEI membrane exhibited robust structural stability, indicating its potential suitability for CO_2 capture from natural gas applications.

3.6. Simulation of industrial environment

To further simulate natural gas industrial conditions, we conducted tests to evaluate the separation performance with feed gas CO_2: CH_4 = 10: 90 at various temperatures and pressures (Table S5 and Table S6). The CO_2 permeability increases with increasing temperature (25-50 °C) at 1 bar (Table S5). The CO_2 permeability reached 2363 Barrer with the selectivity of 19.3 at 50 °C. As shown in Table. S6, when the pressure further increased, the mixed-gas selectivity slightly decreased. The CO_2 permeability remained at 2133 Barrer with CO_2/CH_4 selectivity of 15.1 at 50 °C and 10 bar, proving that the P_{in}@NH_2-UiO-66-PEI membrane has excellent CO_2 permeability. MOFs-based MMMs with mixed CO_2/CH_4 (volume ratio 10/90) reported in the literature are detailed in Table S6, with 30-P_{in}@NH_2-UiO-66-PEI showing superior CO_2 permeability.

Therefore, the high-performance P_{in}@NH_2-UiO-66-PEI membrane holds significant potential for industrial applications.

The 30-P_{in}@NH_2-UiO-66-PEI was subjected to a pressure of 60 bar for 3 hours using a preforming machine to emulate the stability under high-pressure environment. A comparison between the optical photographs and the surface SEM images of the membrane taken before and after the application of pressure (Fig. S9). The membrane's surface retained its initial morphology with some indentations and wrinkles after the pressure exposure. Subsequently, the gas separation efficiency of mixed CO_2/CH_4 (volume ratio 10/90) of this membrane was tested at 50 °C and 10 bar, and the findings indicated that the CO_2/CH_4 separation performance were maintained at a high level (Table. S7).

3.7. Comparison with upper bound

Fig. 11 a shows the CO_2/CH_4 separation performances for the P_{in}@NH_2-UiO-66-PEI, P@NH_2-UiO-66-PEI membranes compared with reported other state-of-the-art functional groups modified MOFs MMMs and 2008 Robeson upper bounds. It can be indicated that CO_2 permeability and CO_2/CH_4 selectivity of P_{in}@NH_2-UiO-66-PEI exhibited significant enhancements compared to other functional group-modified MOFs membranes. Moreover, Fig. 11 b and Table S7 illustrates the comparison of P_{in}@NH_2-UiO-66-PEI and reported other MMMs that were measured with a mixed feed gas of CO_2/CH_4=10/90. The P_{in}@NH_2-UiO-66-PEI membrane stands out due to its exceptionally high CO_2 permeability compared to other membranes. In addition, 30-P_{in}@NH_2-UiO-66-PEI demonstrated enhanced CO_2/CH_4 separation performance, exceeding the upper bound established in 2008, demonstrating the developed membrane with high potentiality for natural gas purification.

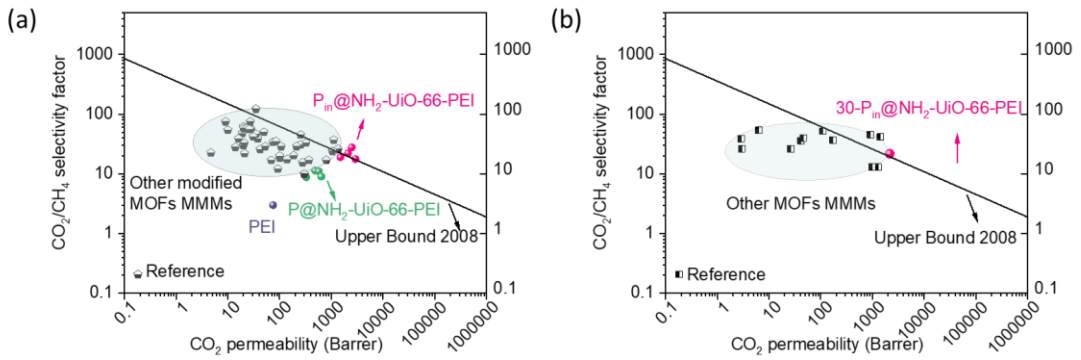

Fig. 11. Contrast of CO_2/ CH_4 separation performances of 30-P_{in}@NH_2-UiO-66-PEI with (a) Robeson upper bound and other modified MOFs based MMMs, (b) other MOFs MMMs in feed gas CO_2/CH_4 =10/90.

Conclusions

In summary, this study reported the synthesis of polyethyleneimine-modified MOF fillers via an in situ one-pot method, and then incorporated into PEI to construct mixed matrix membranes for efficient CO_2/CH_4 separation. The separation performance of as-synthesized MMMs (P_{in}@NH_2-UiO-66-PEI) was also compared with that of MMMs with fillers prepared via conventional wet impregnation method (P@NH_2-UiO-66-PEI). Owing to the presence of polyethyleneimine in the in situ one-pot synthesis, P_{in}@NH_2-UiO-66 fillers have smaller particle size (~20 nm) and higher CO_2 adsorption capacity, improving the interfacial compatibility of MMM and the CO_2 transfer capability. The CO_2 permeability and CO_2/CH_4 selectivity of 30-P_{in}@NH_2-UiO-66-PEI MMMs (30 wt% loading) reached 2498.9 Barrer and 27.7, which were remarkably increased than that of pristine PEI membranes (75.1 Barrer and 3.3, respectively) and P@NH_2-UiO-66-PEI membranes (484.2 Barrer and 11.4, respectively). In addition, we simulated the industrial natural gas purification conditions (50 °C, 10 bar and CO_2: CH_4 = 10: 90 feed gas), and the P_{in}@NH_2-UiO-66-PEI membranes still have CO_2 permeability of 2133 Barrer and CO_2/CH_4 selectivity of 15.1 under these conditions. This study provides a novel perspective on the reasonable design of nano-fillers with unique properties and solve the interfacial compatibility of the MMMs for the development of natural gas purification membranes.

Acknowledgements

This work was supported by the National Natural Science Foundation of China (Grant No. 22175200), National Key Research and Development Program of China of Ministry of Science and Technology (2022YFE010437), Qingdao Municipal Natural Science Foundation of China (23-2-1-240-zyyd-jch), Natural Science Foundation of Shandong Province (ZR2023MB074), and Double Hundred Foreign Experts Plan of Shandong Province (WSR2023056).

References

[1] D. Jiménez-De-La-Cuesta, T. Mauritsen. Emergent constraints on Earth's transient and equilibrium response to doubled CO_2 from post-1970s global warming. Nature Geoscience, 12 (2019) 902-905. https://doi.org/10.1038/s41561-019-0463-y

[2] R. W. Baker, B. Freeman, J. Kniep, X. Wei, T. Merkel. CO_2 capture from natural gas power plants using selective exhaust gas recycle membrane designs. International Journal of Greenhouse Gas Control, 66 (2017) 35-47. https://doi.org/10.1016/j.ijggc.2017.08.016

[3] H. Zhai. Advanced Membranes and Learning Scale Required for Cost-Effective Post-combustion Carbon Capture. iScience, 13 (2019) 440-451. https://doi.org/10.1016/j.isci.2019.03.006

[4] S. Zhou, O. Shekhah, A. Ramírez, P. Lyu, E. Abou-Hamad, J. Jia, J. Li, P. M. Bhatt, Z. Huang, H. Jiang, T. Jin, G. Maurin, J. Gascon, M. Eddaoudi. Asymmetric pore windows in MOF membranes for natural gas valorization. Nature, 606 (2022) 706-712. https://doi.org/10.1038/s41586-022-04763-5

[5] I. Sullivan, A. Goryachev, I. A. Digdaya, X. Li, H. A. Atwater, D. A. Vermaas, C. Xiang. Coupling electrochemical CO_2 conversion with CO2 capture. Nature Catalysis, 4 (2021) 952-958. https://doi.org/10.1038/s41929-021-00699-7

[6] Z. Liu, Y. Liu, W. Qiu, W. J. Koros. Molecularly Engineered 6FDA-Based Polyimide Membranes for Sour Natural Gas Separation. 59 (2020) 14877-14883. https://doi.org/https://doi.org/10.1002/anie.202003910

[7] C. Ma, M. Wang, Z. Wang, M. Gao, J. Wang. Recent progress on thin film composite membranes for CO_2 separation. Journal of CO_2 Utilization, 42 (2020) 101296. https://doi.org/https://doi.org/10.1016/j.jcou.2020.101296

[8] S. Miri, M. Omidkhah, A. Ebadi Amooghin, T. Matsuura. Membrane-based gas separation accelerated by quaternary mixed matrix membranes. Journal of Natural Gas Science and Engineering, 84 (2020) 103655. https://doi.org/10.1016/j.jngse.2020.103655

[9] R. W. Baker, B. T. Low. Gas Separation Membrane Materials: A Perspective. Macromolecules, 47 (2014) 6999-7013. https://doi.org/10.1021/ma501488s

[10] G. Liu, A. Cadiau, Y. Liu, K. Adil, V. Chernikova, I.-D. Carja, Y. Belmabkhout, M. Karunakaran, O. Shekhah, C. Zhang, A. K. Itta, S. Yi, M. Eddaoudi, W. J. Koros. Enabling Fluorinated MOF - Based Membranes for Simultaneous Removal of H_2S and CO_2 from Natural Gas. Angew Chem Int Ed, 57 (2018) 14811. https://doi.org/10.1002/anie.201808991

[11] X. Cai, Y. Yuan, M. Sheng, J. Wang, Z. Wang. High-performance CO_2/CH_4 separation membrane fabrication with PVAm modified by the MOFs containing amine groups. Journal of Natural Gas Science and Engineering, 89 (2021) 103874.

https://doi.org/10.1016/j.jngse.2021.103874

[12] M. Costa Flores, K. C. D. S. Figueiredo. Asymmetric oxygen-functionalized carbon nanotubes dispersed in polysulfone for CO_2 separation. J Appl Polym Sci, 140 (2022). https://doi.org/10.1002/app.53303

[13] C. Wu, K. Zhang, H. Wang, Y. Fan, S. Zhang, S. He, F. Wang, Y. Tao, X. Zhao, Y. B. Zhang, Y. Ma, Y. Lee, T. Li. Enhancing the Gas Separation Selectivity of Mixed-Matrix Membranes Using a Dual-Interfacial Engineering Approach. J Am Chem Soc, 142 (2020) 18503-18512. https://doi.org/10.1021/jacs.0c07378

[14] R. Ding, Q. Wang, X. Ruan, Y. Dai, X. Li, W. Zheng, G. He. Novel and versatile PEI modified ZIF-8 hollow nanotubes to construct CO_2 facilitated transport pathway in MMMs. Sep Purif Technol, 289 (2022) 120768. https://doi.org/10.1016/j.seppur.2022.120768

[15] Q. Qian, P. A. Asinger, M. J. Lee, G. Han, K. Mizrahi Rodriguez, S. Lin, F. M. Benedetti, A. X. Wu, W. S. Chi, Z. P. Smith. MOF-Based Membranes for Gas Separations. Chem Rev, 120 (2020) 8161-8266. https://doi.org/10.1021/acs.chemrev.0c00119

[16] B. Chen, C. Wan, X. Kang, M. Chen, C. Zhang, Y. Bai, L. Dong. Enhanced CO_2 separation of mixed matrix membranes with ZIF-8@GO composites as fillers: Effect of reaction time of ZIF-8@GO. Sep Purif Technol, 223 (2019) 113-122. https://doi.org/10.1016/j.seppur.2019.04.063

[17] P. Duan, J. C. Moreton, S. R. Tavares, R. Semino, G. Maurin, S. M. Cohen, K. Schmidt-Rohr. Polymer Infiltration into Metal-Organic Frameworks in Mixed-Matrix Membranes Detected in Situ by NMR. J Am Chem Soc, 141 (2019) 7589-7595. https://doi.org/10.1021/jacs.9b02789

[18] A. R. Nabais, R. Ribeiro, J. Mota, V. D. Alves, I. Esteves, L. A. Neves. CO_2/N_2 Gas Separation using Fe(BTC)-based Mixed Matrix Membranes: A view on the adsorptive and filler properties of Metal-Organic Frameworks. Sep Purif Technol, 202 (2018) 174-184. https://doi.org/10.1016/j.seppur.2018.03.028

[19] S. Rafiq, M. Saeed, A. Jamil, M. I. Rashid, M. Irfan, T. Iqbal, A. Inayat, F. Jamil, J. Iqbal, M. S. Khurram, M. S. Mehadi. Advances in Halloysite Nanotubes (HNTs)-Based Mixed-Matrix Membranes for CO_2 Capture. ChemBioEng Reviews, 10 (2023) 480-490. https://doi.org/https://doi.org/10.1002/cben.202200041

[20] C. Song, R. Li, Z. Fan, Q. Liu, B. Zhang, Y. Kitamura. CO_2/N_2 separation performance of Pebax/MIL-101 and Pebax/NH_2-MIL-101 mixed matrix membranes and intensification via sub-ambient operation. Sep Purif Technol, 238 (2020) 116500. https://doi.org/10.1016/j.seppur.2020.116500

[21] S. Mutyala, M. Jonnalagadda, S. M. Ibrahim. Effect of modification of UiO-66 for CO_2 adsorption and separation of CO_2/CH_4. J Mol Struct, 1227 (2021) 129506. https://doi.org/10.1016/j.molstruc.2020.129506

[22] C. Ma, J. J. Urban. Hydrogen-Bonded Polyimide/Metal-Organic Framework Hybrid Membranes for Ultrafast Separations of Multiple Gas Pairs. Advanced Functional Materials, 29 (2019). https://doi.org/10.1002/adfm.201903243

[23] A. Atash Jameh, T. Mohammadi, O. Bakhtiari. Preparation of PEBAX-1074/modified ZIF-8 nanoparticles mixed matrix membranes for CO_2 removal from natural gas. Sep Purif Technol, 231 (2020) 115900. https://doi.org/10.1016/j.seppur.2019.115900

[24] A. Jomekian, B. Bazooyar, R. M. Behbahani, T. Mohammadi, A. Kargari. Ionic liquid-modified Pebax® 1657 membrane filled by ZIF-8 particles for separation of CO_2 from CH_4, N_2 and H_2. J Membr Sci, 524 (2017) 652-662. https://doi.org/10.1016/j.memsci.2016.11.065

[25] M. Mirkovic, M. S. Yilmaz, L. Kljajevic, V. Pavlovic, M. Ivanovic, D. Djukic, T. Eren. Design of PEI and Amine Modified Metakaolin-Brushite Hybrid Polymeric Composite Materials for CO_2 Capturing. Polymers, 15 (2023). https://doi.org/10.3390/polym15071669

[26] X. Wang, Y. Wang, Y. Shan, X. Wang, Y. Yang, F. Zhang, X. Chen. Polyethyleneimine-modified multi-walled carbon nanotubes mixed matrix membranes for CO_2/N_2 separation. Journal of Environmental Chemical Engineering, 11 (2023) 109537. https://doi.org/https://doi.org/10.1016/j.jece.2023.109537

[27] W. Wu, Z. Li, Y. Chen, W. Li. Polydopamine-Modified Metal-Organic Framework Membrane with Enhanced Selectivity for Carbon Capture. Environ Sci Technol, 53 (2019) 3764-3772. https://doi.org/10.1021/acs.est.9b00408

[28] J. Zhu, L. Wu, Z. Bu, S. Jie, B.-G. Li. Polyethyleneimine-Modified UiO-66-NH_2(Zr) Metal–Organic Frameworks: Preparation and Enhanced CO_2 Selective Adsorption. ACS Omega, 4 (2019) 3188-3197. https://doi.org/10.1021/acsomega.8b02319

[29] Q. Zhao, Y. Sun, J. Zhang, F. Fan, T. Li, G. He, C. Ma. Mixed matrix membranes incorporating amino-functionalized ZIF-8-NH_2 in a carboxylic polyimide for molecularly selective gas separation. Journal of Membrane Science, 693 (2024). https://doi.org/10.1016/j.memsci.2023.122326

[30] X. Guo, L. Ding, K. Kanamori, K. Nakanishi, H. Yang. Functionalization of hierarchically porous silica monoliths with polyethyleneimine (PEI) for CO_2 adsorption. Microporous Mesoporous Mater, 245 (2017) 51-57. https://doi.org/10.1016/j.micromeso.2017.02.076

[31] Y. Zhou, Y. Wang, Y. Wang, X. Li. Humidity-Enabled Ionic Conductive Trace Carbon Dioxide Sensing of Nitrogen-Doped $Ti_3C_2T_x$ MXene/Polyethyleneimine Composite Films Decorated with Reduced Graphene Oxide Nanosheets. Anal Chem, 92 (2020) 16033-16042. https://doi.org/10.1021/acs.analchem.0c03664

[32] B. Liu, D. Li, J. Yao, H. Sun. Enhanced CO_2 selectivity of polyimide membranes through dispersion of polyethyleneimine decorated UiO-66 particles. J Appl Polym Sci, 137 (2020). https://doi.org/10.1002/app.49068

[33] B. Liu, D. Li, J. Yao, H. Sun. Improved CO_2 separation performance and interfacial affinity of mixed matrix membrane by incorporating UiO-66-PEI@[bmim][Tf_2N] particles. Sep Purif Technol, 239 (2020) 116519. https://doi.org/10.1016/j.seppur.2020.116519

[34] A. Micero, T. Hashem, H. Gliemann, A. Leon. Hydrogen Separation Performance of UiO-66-NH_2 Membranes Grown via Liquid-Phase Epitaxy Layer-by-Layer Deposition and One-Pot Synthesis. Membranes (Basel), 11 (2021). https://doi.org/10.3390/membranes11100735

[35] Z. Li, W. Zhang, M. Tao, L. Shen, R. Li, M. Zhang, Y. Jiao, H. Hong, Y. Xu, H. Lin. In-situ growth of UiO-66-NH2 in porous polymeric substrates at room temperature for fabrication of mixed matrix membranes with fast molecular separation performance. Chemical Engineering Journal, 435 (2022). https://doi.org/10.1016/j.cej.2022.134804

[36] H. Molavi, A. Shojaei, S. A. Mousavi. Improving mixed-matrix membrane performance via PMMA grafting from functionalized NH_2–UiO-66. Journal of Materials Chemistry A, 6 (2018) 2775-2791. https://doi.org/10.1039/c7ta10480d

[37] S. Basu, A. Cano-Odena, I. Vankelecom. Asymmetric Matrimid/[$Cu_3(BTC)_2$] mixed-matrix membranes for gas separations. J Membr Sci, 362 (2010) 478-487. https://doi.org/10.1016/j.memsci.2010.07.005

[38] S. Soheili, A. Nakhaei Pour, A. Mohammadi. SAPO-34 synthesis by combinations of structure-

directing agents: Experimental and Monte Carlo simulations studies. Microporous Mesoporous Mater, 317 (2021). https://doi.org/10.1016/j.micromeso.2021.111003

[39] J. Fang, L. Zhang, C. Li. Polyamide 6 composite with highly improved mechanical properties by PEI-CNT grafted glass fibers through interface wetting, infiltration and crystallization. Polymer, 172 (2019) 253-264. https://doi.org/10.1016/j.polymer.2019.03.013

[40] Y. Lin, Q. Yan, C. Kong, L. Chen. Polyethyleneimine incorporated metal-organic frameworks adsorbent for highly selective CO_2 capture. Sci Rep, 3 (2013) 1859. https://doi.org/10.1038/srep01859

[41] Z. B. Zhou, X. H. Han, Q. Y. Qi, S. X. Gan, D. L. Ma, X. Zhao. A Facile, Efficient, and General Synthetic Method to Amide-Linked Covalent Organic Frameworks. J Am Chem Soc, 144 (2022) 1138-1143. https://doi.org/10.1021/jacs.1c12392

[42] Q. Liang, M. Zhang, Z. Zhang, C. Liu, S. Xu, Z. Li. Zinc phthalocyanine coupled with UIO-66 (NH_2) via a facile condensation process for enhanced visible-light-driven photocatalysis. J Alloys Compd, 690 (2017) 123-130. https://doi.org/10.1016/j.jallcom.2016.08.087

[43] S. Diring, S. Furukawa, Y. Takashima, T. Tsuruoka, S. Kitagawa. Controlled Multiscale Synthesis of Porous Coordination Polymer in Nano/Micro Regimes. Chem Mater, 22 (2010) 4531-4538. https://doi.org/10.1021/cm101778g

[44] L. Chen, X. Ren, Y. Li, D. Hu, X. Feng, W. Li. Enhancing interface compatibility of UiO-66-NH2 and polyamide by incorporating dopamine into thin film nanocomposite membranes. J Membr Sci, 654 (2022) 120565. https://doi.org/10.1016/j.memsci.2022.120565

[45] K. Chen, L. Ni, H. Zhang, L. Li, X. Guo, J. Qi, Y. Zhou, Z. Zhu, X. Sun, J. Li. Phenolic resin regulated interface of ZIF-8 based mixed matrix membrane for enhanced gas separation. J Membr Sci, 666 (2023) 121117. https://doi.org/10.1016/j.memsci.2022.121117

[46] G. Yang, Y. Wang, M. Sun, P. Xu, C. Wang, K. Huang, H. Jiang, S. Mintova, H. Guo. Is amino-modification of HKUST-1 in PEI mixed-matrix membranes always favorable to CO_2 separation? Microporous Mesoporous Mater, 359 (2023) 112649. https://doi.org/10.1016/j.micromeso.2023.112649

[47] A. Choudhury. Dielectric and piezoelectric properties of polyetherimide/$BaTiO_3$ nanocomposites. Mater Chem Phys, 121 (2010) 280-285. https://doi.org/10.1016/j.matchemphys.2010.01.035

[48] Y. Wang, G. Yang, H. Guo, X. Meng, G. Kong, Z. Kang, R. Guillet-Nicolas, S. Mintova. Preparation of HKUST-1/PEI mixed-matrix membranes: Adsorption-diffusion coupling control of small gas molecules. J Membr Sci, 643 (2022) 120070. https://doi.org/10.1016/j.memsci.2021.120070

[49] E. D. Walter, D. Zhang, Y. Chen, K. Sung Han, J. D. Bazak, S. Burton, K. O'harra, D. W. Hoyt, J. E. Bara, D. Malhotra, S. I. Allec, V. A. Glezakou, D. J. Heldebrant, R. Rousseau. Enhancing CO_2 Transport Across a PEEK-Ionene Membrane and Water-Lean Solvent Interface. ChemSusChem, 16 (2023) e202300157. https://doi.org/10.1002/cssc.202300157

[50] Z. Dai, L. Deng. Membrane absorption using ionic liquid for pre-combustion CO_2 capture at elevated pressure and temperature. International Journal of Greenhouse Gas Control, 54 (2016) 59-69. https://doi.org/10.1016/j.ijggc.2016.09.001